Surveys in Geophysics
https://doi.org/10.1007/s10712-026-09933-y

Deployment of a Dense Seismic Network on La Palma Island (2023-2024) for High-Resolution Imaging of the Velocity Structure Using Passive Seismic Methods

Javier Tortosa[1,2] · Javier Almendros[1,2] · Enrique Carmona[2] · José Benito Martín[2] · Janire Prudencio[1,2] · Joan Antoni Parera-Portell[1,2] · Rafael Abella[3] · Carlos Araque-Pérez[1,2] · José Morales[1,2] · Pablo Rey-Devesa[1,2] · Benjamin Heit[4] · Xiaohui Yuan[4] · Alfonso Ontiveros-Ortega[5] · Iván Melchor[6] · Cinthia Guerrero-Reinoso[1,2] · David Carrero[2] · Inmaculada Serrano[1,2] · Gerardo Alguacil[1,2] · Guillermo Cortés[1,2] · Mercedes Feriche[2] · Antonio Martos[2] · Javier Moreno[2] · Miguel Ángel Dengra[2]

Received: 20 May 2025 / Accepted: 15 January 2026
© The Author(s) 2026

Abstract
We present the IMAGMASEIS project, a large-N seismic experiment carried out on La Palma (Canary Islands, Spain) between 2023 and 2024, aimed at high-resolution imaging of the crustal and upper mantle structure using passive seismic methods. The project involved the deployment of 235 temporary broadband and short-period seismic stations, supplementing 21 permanent stations, thus creating the densest seismic network ever installed on the island. The main goal is to characterise the magmatic plumbing system beneath Cumbre Vieja volcano, identify magma accumulation zones, and investigate structural changes related to the 2021 Tajogaite eruption. We describe the experimental design, network configuration, instrumentation, deployment strategies, and challenges encountered, including difficult terrain and logistical constraints. Preliminary results demonstrate the potential of the dataset for ambient noise tomography, receiver function analysis, and local earthquake studies. IMAGMASEIS provides a valuable resource for understanding volcanic and tectonic processes in oceanic island settings and serves as a model for cost-effective, high-density seismic deployments in similar environments.

Keywords Seismic network · Large-N deployment · Seismic Imaging · Magma plumbing system · La Palma · Canary Islands

Article Highlights

- The densest seismic network ever deployed on La Palma to study underground structures

Extended author information available on the last page of the article

- The new data will help identify magma storage areas beneath the Cumbre Vieja volcanic ridge
- The project establishes a model for high-density, low-cost seismic deployments on volcanic islands

1 Introduction

The island of La Palma (Fig. 1) is the youngest of the Canary Islands, Spain. This island began to form about 4 Ma ago with the creation of a submarine volcano which, after emerging on the surface, gave way to a succession of two volcanic edifices interspersed by large landslides: the Garafía edifice (1.8−1.2 Ma ago) and the Taburiente edifice (1.1−0.4 Ma ago). During the last stages of the Taburiente volcano, activity shifted southwards, culminating in the Cumbre Nueva edifice, which suffered a new large landslide 560 ka ago. This landslide exposed part of the submarine volcano and the Garafía edifice, creating the Caldera de Taburiente, which shapes the characteristic topography of the island. The Bejenado volcano (0.56 - 0.49 Ma) emerged on the deposits of this landslide (Carracedo et al. 2001).

After a period of inactivity, volcanic activity migrated southwards again 123 ka ago, creating the Cumbre Vieja edifice, the most active volcanic field in the Canary Islands. This edifice is a north–south-oriented ridge about 20 km long and with a maximum elevation of about 1950 m.a.s.l. All recent eruptions in La Palma took place at Cumbre Vieja, with 7 eruptions occurring since historical records are kept on the area (~1493 AD) (Troll and Carracedo 2016). Two of these eruptions occurred in the twentieth century, the San Juan eruption in 1949 and the Teneguía eruption in 1971. The San Juan eruption was preceded by years of seismic activity and produced three eruptive vents in the central area of Cumbre Vieja (Romero Ruiz 1990). The Teneguía eruption was also preceded by days of intense seismicity and originated as a fissure near a phonolitic dome at the southern part of the island (Troll and Carracedo 2016).

Since 1971, Cumbre Vieja remained quiet for 46 years, until October 2017, when there were some clusters of deep earthquakes. This was the first evidence of magmatic reactivation (Torres-González et al. 2020). The seismic swarms continued sporadically until August 2021, with hypocentres located at a depth of about 20 km. On 11 September 2021, a new seismic swarm started at a depth of 10 km beneath the eastern slopes of Cumbre Vieja (Del Fresno et al. 2023). In the following days, seismicity migrated westwards and ascended, and ground deformation began to be detected. The process culminated on 19 September with the eruption of Tajogaite volcano, which lasted until 13 December (85 days). The eruption had a mixed character, both explosive and effusive, resulting in the formation of cinder cones and lava flows, which were emplaced over a very large area causing great damage to infrastructure and buildings, as well as the emission of a large amount of gases and ash (Martí et al. 2022). During the eruption, two earthquake clusters were observed, located at approximately 10 and 25 km depth beneath Cumbre Vieja (D'Auria et al. 2022). After the eruption, residual activity at Tajogaite has been documented as small seismic events (Tortosa 2023), continuous degassing, and high surface temperatures.

Prior to the 2021 eruption, only a few geophysical studies had been published about La Palma. Some of the existing research includes gravity measurements (Camacho et al. 2009), geodesy (Prieto et al. 2009), magnetotellurics (Di Paolo et al. 2020), and seismicity analyses (Torres-González et al. 2020). However, following the Tajogaite eruption,

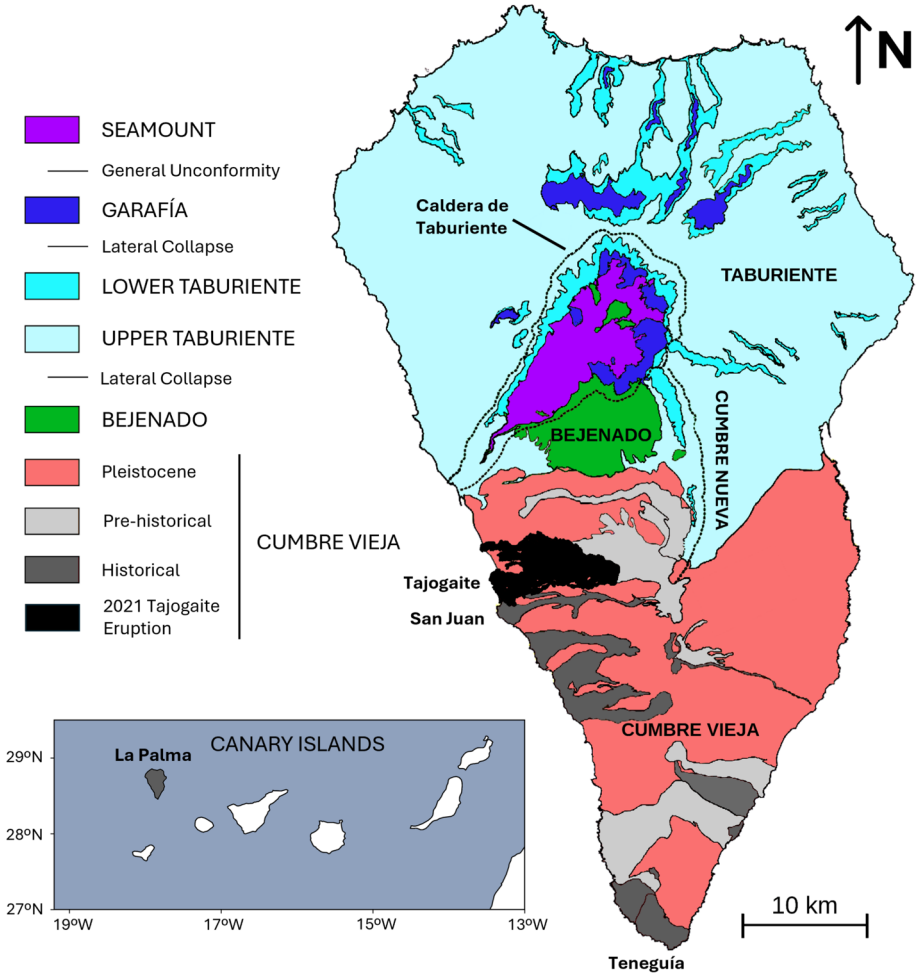

Fig. 1 Geological map of La Palma showing the stratigraphic units and lava flows from the Cumbre Vieja volcano (modified after Troll and Carracedo 2016). The contour of the 2021 lava flow is based on data from Civico et al. (2022)

numerous studies have been carried out. Some of them focus on understanding the eruptive stages and processes (D'Auria et al. 2022; Del Fresno et al. 2023; Longpré et al. 2025), while others also aim to improve our knowledge about the internal structure of the island (Day et al. 2022; Dayton et al. 2023; Przeor et al. 2024; Rodríguez-Pascua et al. 2024; Romero-Toribio et al. 2025). These include seismological methods using data obtained before and during the eruption such as local earthquake seismic tomography (D'Auria et al. 2022; Serrano et al. 2023; Gammaldi et al. 2025), receiver function analysis (Ortega-Ramos et al. 2024), ambient noise velocity (Cabrera-Pérez et al. 2023), and attenuation tomography (Cabrera-Pérez et al. 2024). Although these seismic studies have provided valuable insights, their scope has been influenced by the number and distribution of seismic stations available, which, in some cases, limits the ability to achieve high-resolution imaging across the entire island. This raised the necessity to perform a large-scale, high-density

seismic deployment covering the entire island to obtain results with a greater extent and resolution, to perform studies of the variations in the internal structure, and to characterise the changes produced after the eruption.

During the last decades, several large-N seismic deployments have been carried out at different scales that have inspired our experiment. We can mention the USArray (Meltzer et al. 1999), IberArray (Díaz et al. 2009), and AlpArray (Hetényi et al. 2018), all of them using broadband seismometers, as well as other experiments involving short-period geophones e.g., (Hansen and Schmandt, 2015; Ryberg et al., 2022; Lin et al., 2013; Liu et al., 2017). In this context, we devised a research project entitled "**Imag**ing the **ma**gmatic plumbing system of Cumbre Vieja volcano using passive **seis**mological methods" (IMAGMASEIS) as a large-N seismic experiment focused on characterising the seismic structure of La Palma island. The project included the deployment of 235 broadband and short-period seismic stations (Almendros et al. 2023) that were temporarily added to the 21 permanent broadband stations operated by the Instituto Geográfico Nacional (1999) and the Instituto Volcanológico de Canarias (2016).

The main goal of the IMAGMASEIS project is to understand the crustal and upper mantle structure, as well as the tectonic regime in La Palma. This involves imaging the magmatic plumbing system of Cumbre Vieja, identifying the magma accumulation zones beneath it, and determining their sizes, depths, and interconnections between them. In particular, we intend to image the magma source that fed the 2021 eruption and if there are other areas susceptible to develop vents in the near future. In addition, the project aims to obtain an image of the topography of the Moho and address questions such as the possible presence of an underplating layer beneath La Palma. To achieve these results, several seismological methods will be applied, including ambient noise tomography, receiver function analysis, local earthquake studies, travel-time tomography, SKS splitting analysis, and attenuation tomography, among others. The design of the experiment was carried out with the aim of obtaining a high resolution with these methods.

In this paper, we show an overview of the project, including the deployments made, the challenges encountered, and a description of the characteristics of the data obtained. We also show some preliminary results that demonstrate the potential applications of this dataset.

2 Experimental Setup

2.1 Seismic Instruments

For this experiment, we had a set of instruments comprising 35 broadband seismometers, 200 short-period geophones, and 235 data acquisition systems. Broadband seismometers were mostly Nanometrics Trillium Compact, except for 5 seismometers that were Trillium Compact Posthole. All of them had a natural period of 120 s and a sensitivity of 754 V/(m/s). Short-period seismometers were Sensor Nederland PE-6B instruments, with a natural frequency of 4.5 Hz. Acquisition systems were mostly Digos Datacube3, except for 3 Nanometrics Centaur dataloggers. The instruments were provided by the GFZ through the GIPP pool (20 Trillium Compact, 200 geophones, 230 Datacube3) and by the University of Granada (10 Trillium Compact, 5 Posthole, 3 Centaur, 2 Datacube3).

The broadband seismometers were buried at a depth of 50-60 cm. They were located on a thick concrete slab and covered with foamed polystyrene to insulate them from

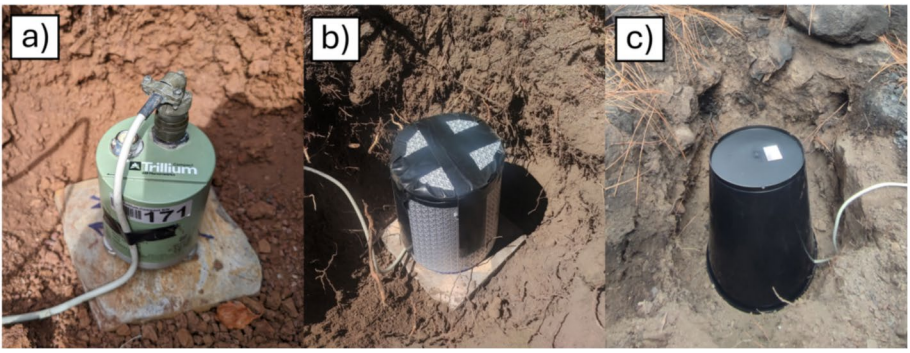

Fig. 2 Broadband sensor installation. **a** Sensor over the concrete slab in a hole of 50-60 cm depth, levelled and oriented to the north. **b** Foamed polystyrene cover to insulate the sensor from temperature changes and air currents. **c** Plastic bucket to protect the seismometer

Fig. 3 Short-period sensor installation. Sensor nailed to the ground in a hole of 10-15 cm depth, levelled and oriented to the north

temperature changes and air currents. Then, we added a plastic bucket to protect the seismometer (Fig. 2) and buried the ensemble filling the hole to the ground level. The short-period sensors are less sensitive to external conditions so they were buried at depths of about 10 cm (Fig. 3). All seismometers were levelled using the built-in bubble and oriented to the north using a compass.

All stations were designed to run for long periods of time without being serviced. This is a crucial point in projects involving a large number of stations on a limited budget (Heit et al. 2021). For this reason, power supply was provided by zinc/air batteries. This type of slow-discharge battery is designed to provide a small current over a long time, as opposed to standard car batteries that have to provide relatively large current pulses. Therefore, they are best suited for use with seismometers in field deployments. Additionally, with a sufficient number of battery cells we can obtain power supply for long periods of time (on the order of months and years), so continuous recharge with solar panels is not required, greatly simplifying the deployments. In our deployments, we followed the recommendations of Heit et al. (2021).

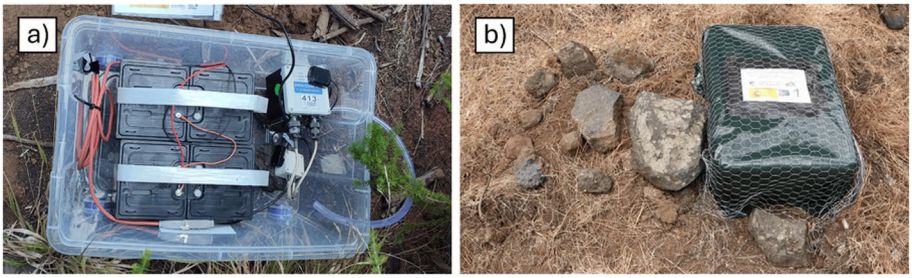

Fig. 4 Broadband station installation. **a** Plastic box containing two zinc/air batteries, the datalogger, breakout box, GPS antenna, cables and a plastic tube for ventilation. **b** Final aspect of the seismic station. The seismometer is buried under the rocks on the left. The plastic box is partially buried and covered with dark green raffia and chicken wire to protect the station and reduce the visual impact

The zinc/air batteries are sensitive to low temperature and high humidity conditions, so we placed them with the dataloggers in plastic boxes (Fig. 4a). These boxes had holes at the bottom to evacuate any water that could enter during rain episodes or condensate from ambient humidity. Another hole close to the top allowed for the passage of a small plastic tube for the ventilation of the batteries. This is a requirement, since zinc/air batteries need a constant air flow for adequate performance. The plastic boxes were partially buried and covered with dark green raffia and chicken wire to protect them from animals, rain, and other potential hazards (Fig. 4b).

Most of the broadband stations were equipped with Datacube3 dataloggers and Trillium Compact seismometers. Exceptions were two stations with Datacube3 dataloggers and Trillium Compact Posthole seismometers, and three stations with Centaur dataloggers and Trillium Compact Posthole (see Table S1). The Datacube3 dataloggers were configured with gain 8 and a sampling rate of 100 sps. Internal time was synchronised by GPS every 51 min. In this configuration, the output voltage of the Trillium Compact is reduced by a factor of 1/10 via a breakout box. The Centaur dataloggers were configured with gain 1 (one of them with gain 2, see Table S1), continuous GPS synchronisation, and a sampling rate of 100 sps. The broadband stations using Datacube3 dataloggers were powered by two zinc/air batteries CEGASA E/Z8 9/400, connected in series to provide 360 Ah at 18 V, which we calculated to be sufficient for a period of 14 months. The Centaur dataloggers, given their larger power consumption, were installed only at locations with an available connection to the power grid. A small car battery connected to a battery charger was then sufficient to ensure the continuous operation of the stations.

Short-period stations were also equipped with Datacube3 dataloggers. In this case, they were configured with gain 16. Sampling was adjusted at 100 sps except for some instruments deployed densely near the volcano edifice (TJ stations, see Table S1) which were set at 200 sps. Again, internal time was synchronised by GPS every 51 min. Power was supplied by one zinc/air battery CEGASA E/Z8 9/200, providing 180 Ah at 9 V (Fig. 5), which would ensure 8 months of continuous operation.

2.2 Deployments and Field Operations

The experiment started in June 2023 with a general survey of the island, intended to get a first-hand overview of the different areas of La Palma. We travelled around the island

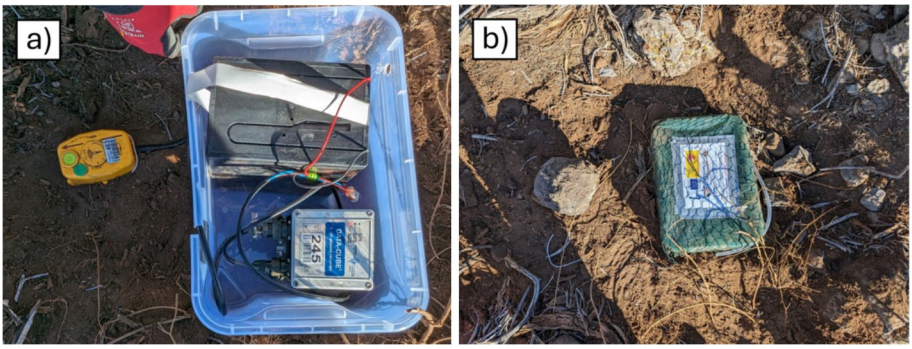

Fig. 5 Short-period station installation. **a** Plastic box containing one zinc/air battery, the datalogger (with internal GPS antenna), cables, and a plastic tube for ventilation. **b** Final aspect of the seismic station. The geophone is buried under the rock on the left. The plastic box is partially buried and covered with dark green raffia and chicken wire to protect the station and reduce the visual impact

for a week to know the roads and pathways, their accessibility, the type of terrain, and contacts required for access. We also installed the first broadband station (BB23). The bulk deployment of the seismic stations of the IMAGMASEIS project took place over three main campaigns in September 2023, February 2024, and June 2024. All instruments were removed in October 2024.

The first deployment took place in September 2023, when we performed the installation of the broadband instruments (BB network, Fig. 6a). The deployment was carried out by a group of 6 people in a time period of 8 days. This network consisted of 35 broadband seismometers that were distributed uniformly throughout the island to obtain good coverage of the entire study area. To optimise the deployment, we took into account the locations of the permanent stations already installed by IGN and INVOLCAN. In this way, a dense network

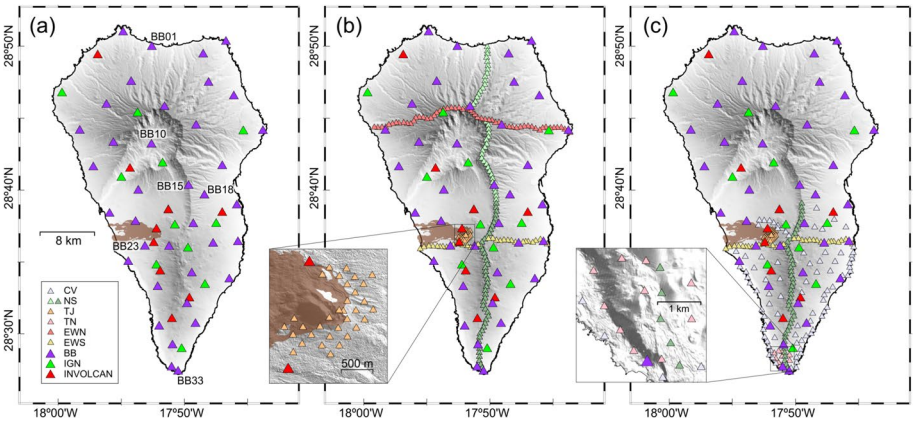

Fig. 6 Map of the seismic instruments deployed during the IMAGMASEIS experiment, including the permanent seismic networks of IGN and INVOLCAN. The three panels show the stations operating during the periods (a) September 2023 to February 2024 (**a**); February to June 2024 (**b**); and June to October 2024 (**c**). The insets zoom in the areas around Tajogaite and Teneguía. The brown area is the lava field from the 2021 eruption. In the (a) panel stations used for Fig. 10 are labelled

of broadband seismometers was achieved. In all cases, the distance from each station to the nearest station was less than 5 km. Since one of the Trillium Compact seismometers failed during deployment in September 2023, only stations BB01 through BB34 were initially deployed. In January 2024, we carried out a campaign by 4 persons during 9 days to collect the data from this network and to find locations for the next deployments. We also removed the station BB02, due to a requirement of the land owner, and redeployed it as station BB35 at the NE tip of the island. We also deployed the repaired instrument as station BB36. In June 2024, we redeployed this station in the northern end of the island as station BB37 to improve the coverage in this area. The BB network was operational until the end of October 2024, recording a total of 13 months of data (Figs. 7 and S1). Station BB23 was actually deployed during the exploration survey (June 2023) so its data span three extra months.

The second deployment was carried out by 10 people during 2 weeks in February 2024. A total of 200 short-period geophones were installed in 4 different sub-networks (Fig. 6b). Three of them consisted of linear profiles with an average inter-station distance of 500 m. The NS profile extended from north to south, with 84 stations covering a total distance of 41.4 km. The WN network was an east–west profile in the northern part of the island, with 55 stations covering a length of 23.3 km. The WS network was also an east–west profile located in the central part of the island, across the 2021 eruption site, with 29 stations along 16.4 km. Finally, the TJ network was a very high-density deployment around the Tajogaite edifice. This sub-network was composed of 32 short-period stations in a regular grid configuration with inter-station distances of 200 m and a maximum aperture of 1.8 km. The TJ stations surround the volcano except for the western part, where lava flows are emplaced and therefore no instruments could be installed. The northern half of the NS profile (NS01-NS39) and the WN profile operated until June 2024 (4 months), while the southern part of the NS profile (NS40-NS84), the WS profile, and the TJ network remained in operation for 8 months, until the end of the experiment in October 2024 (Fig. 7). Due to several operational issues, we conducted a short maintenance campaign in April 2024 by 3 people during 5 days.

The last deployment survey was carried out by 10 people in different groups along 21 days in June 2024. The survey consisted of the data collection of all the stations and the relocation of some of the short-period stations. Specifically, we relocated the northern part

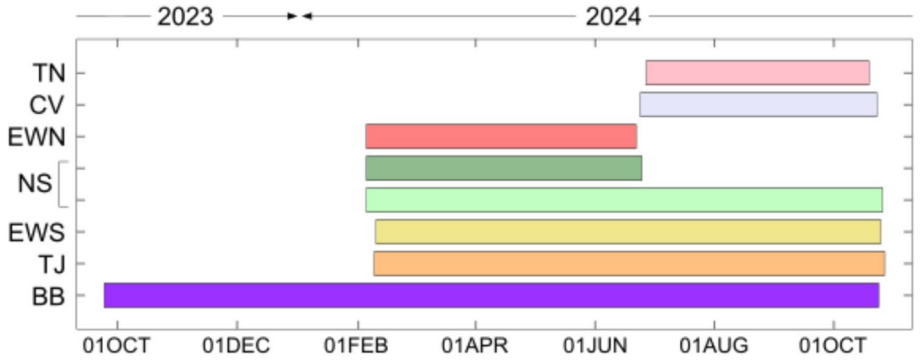

Fig. 7 Periods of operation of the different sub-networks (BB, CV, NS, TJ, TN, EWN, EWS) deployed during the IMAGMASEIS experiment. Detailed information about the operation periods for individual stations can be found in Figure S1 and Table S1

of the NS profile and the WN profile in the southern part of the island, to densify the station coverage in Cumbre Vieja during the final part of the experiment. This new configuration involved the installation of two sub-networks (Fig. 6c). The CV network consisted of 88 short-period stations distributed in the southern half of the island, with a higher density along the coast of the island, forming a ring of stations around the Cumbre Vieja volcanic edifice. In addition, we deployed a small sub-network of 10 stations (TN network) around the Teneguía volcano, which erupted in 1971. Both networks were operational during 4 months, until the end of the study in October 2024 (Fig. 7).

Finally, all instruments were removed in a survey carried out by 11 people in different shifts during 16 days in October 2024. We recovered all elements of the stations, including the seismometers, dataloggers, cables, batteries, plastic boxes, etc., so that we left no environmental impact at the deployment sites. All instruments were cleaned and packed for transportation to University of Granada and GFZ, and the batteries and plastics were sent to a recycling facility in La Palma.

2.3 Challenges

Developing such a high-density experiment on an island with the characteristics of La Palma has posed numerous challenges. La Palma is a relatively small island with a surface area of 708.32 km^2. It has a very complex topography, full of steep slopes, cliffs, and high altitudes reaching 2426 m.a.s.l. at its highest peak (Roque de los Muchachos). This complicates the installation of stations in the configurations proposed in this study, especially in the profiles where a distance between stations of 500 m was desired, which allows a very small margin of error. Although the result obtained in the distribution of the installed stations was very satisfactory, it had to be modified from the initial proposal for this reason.

In addition to the island's complex topography, there are two other important problems. On the one hand, the absence of roads or tracks in the central part of the island meant that about one-third of the deployments (104 in total) had to be accessed on foot, using the local network of trails and paths. Therefore, the installation of these stations required more time than for the others, as they often implied long hikes carrying a large amount of weight at altitudes above 1500 m.a.s.l. For this purpose, groups of three people were formed. Each person carried two complete stations, which allowed the installation of six stations per group and day. When possible, a support group dropped the teams off in accessible areas at high altitude and picked them up at the end of the trail in lower areas, which greatly facilitated the work.

On the other hand, La Palma is very populated in the areas close to the coast. Most of these areas are buildings, plantations, or private homes, making it very difficult to find quiet and adequate locations for the installation of seismic stations. For this reason, local councils were contacted for support and advice. In many cases, they provided locations or contacts where the stations could be installed, but in other cases it was necessary to spend a lot of time looking for locations and neighbours who would accept the installation of the stations on their property. In the end, thanks to the collaboration of authorities and neighbours, it was possible to cover these areas with densities similar to those initially proposed.

Another challenge encountered during installation was how to camouflage the stations to prevent theft or vandalism. Many stations had to be installed near frequented trails. The complex topography limited our ability to set them away from the trails. To solve this

Fig. 8 Camouflage examples of the stations to reduce the visual impact of the stations located in natural spaces and to protect them from possible vandalism

problem, the boxes containing the dataloggers and batteries were partially buried and covered with foliage and dirt to make them as inconspicuous as possible (Fig. 8). The purpose of this operation was to reduce the visual impact of stations located in natural spaces and to protect them from possible vandalism. In any case, we ensured that the camouflage cover was mild enough for the GPS to work properly. This method proved to be satisfactory, as of the 235 stations installed, only one seismic station (CV30) was stolen and another one (BB17) was vandalised (GPS theft). In any case, we acknowledge the high level of awareness among the people of La Palma regarding the risks of living in a volcanic environment. Their respect for scientific instruments and their understanding of their importance undoubtedly contributed to the preservation of the stations throughout the study.

We also found problems due to weather conditions, such as strong winds, rains, and fogs, which complicated the installation in some moments. The weather is very changeable in La Palma and can be completely different in each part of the island. Sometimes, weather conditions can be severe locally, causing problems such as landslides. In fact, one of our stations (BB04) was inaccessible for 7 months due to a huge landslide on the road leading to the station. The delay in servicing the station almost caused it to run out of memory. On days after heavy rains, we encountered lots of rocks on the tracks, which meant delays because of the time required to clean the track and get through with the vehicles.

3 Instrument Performance

3.1 Data Completeness

The performance of the seismic stations during the IMAGMASEIS experiment has been generally satisfactory. The broadband instruments operated for approximately 385 days per station, and we retrieved data for 343 days on average, which represents 89% of the total operating time. Similarly, the short-period stations operated for approximately 253 days per station, and we retrieved data for 245 days on average (97% of the total). These percentages are high, especially for the short-period stations, which indicates that the amount of data lost during the experiment has been very limited.

The power supply provided by the zinc/air batteries had been properly calibrated to the duration of the experiment. Perhaps the calculations fell a bit short in the case of broadband

stations, given that about one-third of the stations ended their operation due to low power supply, days to weeks before the planned recovery (yellow boxes in Figure S1). In the case of short-period instruments, barely 15 out of 200 stations had an early termination related to the power supply.

At some stations of the BB network, we have had problems with channel saturation. This problem occurred for seven different instruments (cyan boxes in Figure S1), although it has been especially severe at stations BB03, BB07, BB09, BB13, and BB21. In some cases, channel saturation could have been driven by ground tilt. The nominal tilt tolerance of the Trillium Compact seismometers is $\pm$ 2.5°. Some seismometers might have become tilted during operation, probably due to mass movements related to rain periods. With increasing tilt, the seismometers (especially their horizontal channels) show a slowly drifting baseline that eventually reaches saturation and makes the data unusable. For stations BB03 and BB21, the re-installation of the seismometer solved the problem. Nevertheless, in other instances the problem seemed to be internal to the instrument and could not be corrected by levelling. These were the cases of stations BB07, BB09, and BB13. This last station was prematurely removed in June 2024 for this reason.

Some instruments were initially deployed at one location and then moved to a different location, for different reasons. For example, station TJCC was deployed near the slopes of Tajogaite, at a location with a high thermal gradient. After a few days, considering the safe functioning of the station during the upcoming months, we decided to move it to a slightly further location as station TJ15. Similarly, stations CV22, CV50, and CV88 were deployed at some initial locations but were immediately relocated following the suggestions of the land owners. Station CV22 was changed to CV84; station CV50 was moved to CV55; and station CV88 was used as station CV60/63.

We have also suffered some problems related to external causes. For example, one short-period station (CV30) was stolen between July and October 2024. Another short-period station (EWS04) was accidentally removed by machinery during construction works at the end of March 2024, although fortunately it could be recovered in good health and their components were redeployed in other locations (CV16/27). Also, the GPS antenna of the BB17 station was cut at the beginning of October 2024. Finally, we found that station CV75 was flooded, probably due to an incorrect closing of the protection box after the casual opening by some inquisitive passer-by.

In just a few cases, we have lost data due to instrumental problems in the Datacube3 dataloggers. These problems include malfunctions of the datalogger and timing problems related to GPS data acquisition. In general, these are minor problems, in the sense that they occurred just in 12 instances out of the 235 stations deployed, which means that the instruments were generally reliable and displayed an excellent performance.

3.2 Seismometer Orientations

The stations were orientated towards the north using magnetic compasses. The possible small movements when they were buried can lead to small deviations of the real sensor orientations with respect to the north. Magnetic declination in La Palma at the time of the experiment was about -4.5°, which is within the expected uncertainty of the manual orientations.

We have used the python code DLOPy (Doran and Laske 2017) to determine the orientations of the broadband sensors. This routine analyses the arrival of teleseismic Rayleigh waves recorded at the stations. It is based on the cross-correlation between the

radial component and the Hilbert transform of the vertical component, optimising the selection of analysis windows by means of modern seismic dispersion maps. A total of 465 teleseismic events with magnitudes greater than 5.5 Mw were selected, with a good distribution in distance and back-azimuth.

The estimated orientations of the stations are shown in Fig. 9 and in Table S2.

For most of the stations, we obtain estimates with very low uncertainty (< 5°) and small deviations that basically indicate that the north component is correctly aligned towards the north. The only station for which we find a misorientation larger than 10° with small uncertainty is BB17 (~ 13°N). This station was located inside a school in the town of Tazacorte, and therefore, nearby metallic elements could cause the deviation of the compass from north.

In nine cases, we find slightly larger uncertainties of 5° to 10°, with a higher dispersion in the orientations. At stations BB02, BB36, and BB37 these uncertainties can be due to the smaller number of teleseisms included in the analysis, which is related to the shorter recording times (see Figure S1). In other cases, there seem to be problems with the horizontal components over some periods of time (e.g. stations BB04, BB06, BB07, and BB09), which also limits the number of usable teleseisms.

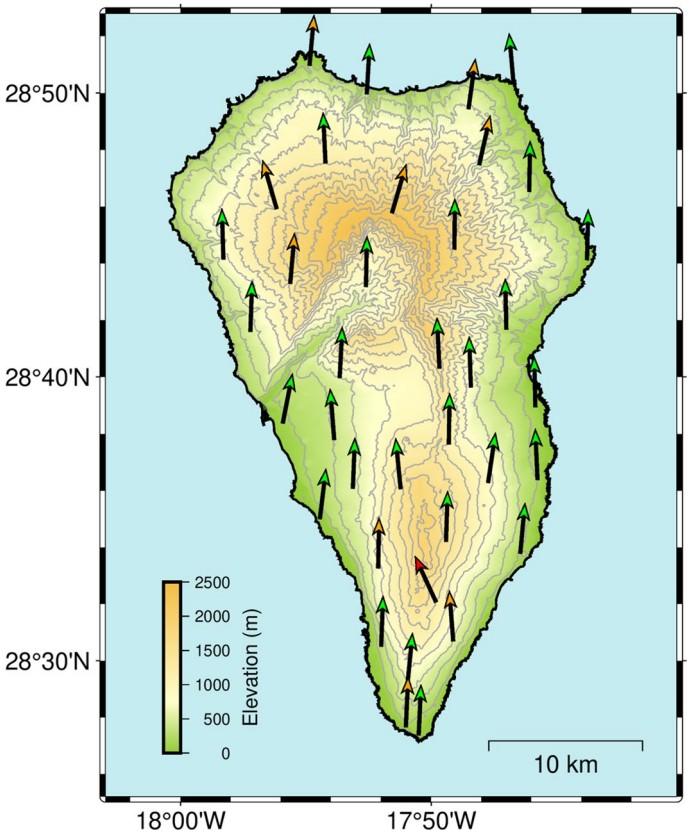

Fig. 9 Orientation of the stations of the BB network. The arrow colours indicate the uncertainty of the estimate: red for large uncertainty (> 10°), orange for intermediate values (5 – 10°), and green for well-constrained orientations (< 5°)

We only find one case (station BB30) in which the uncertainty is so large (~ 40°) that the estimated misorientation of -24.7°N is actually meaningless. This result clearly shows that the station was not working properly.

3.3 Noise Level Analysis

To assess the noise conditions at the stations installed during the project, we performed a spectral analysis using the ISPAQ (IRIS System for Portable Assessment of Quality) software (NSF SAGE 2025). The procedure is based on the calculation of power spectral density (PSD) functions, which allows us to characterise the average noise energy as a function of frequency or period. For each station, probability density function plots (McNamara and Buland 2004) were generated. They provide a visualisation of noise behaviour throughout the study, allowing us to identify both average and extreme conditions. PSDs were calculated from continuous data recorded during the operational period of each station. This tool also allows us to compare the noise conditions with the seismic noise reference models Peterson (1993).

As a representative example, Fig. 10 shows the vertical component of six broadband stations located in different parts of the island. The distributions are generally dominated by the microseismic noise spanning the 1-10 s band. These are mainly secondary microseisms, whereas primary microseisms are of little importance, probably due to the steep drop of the

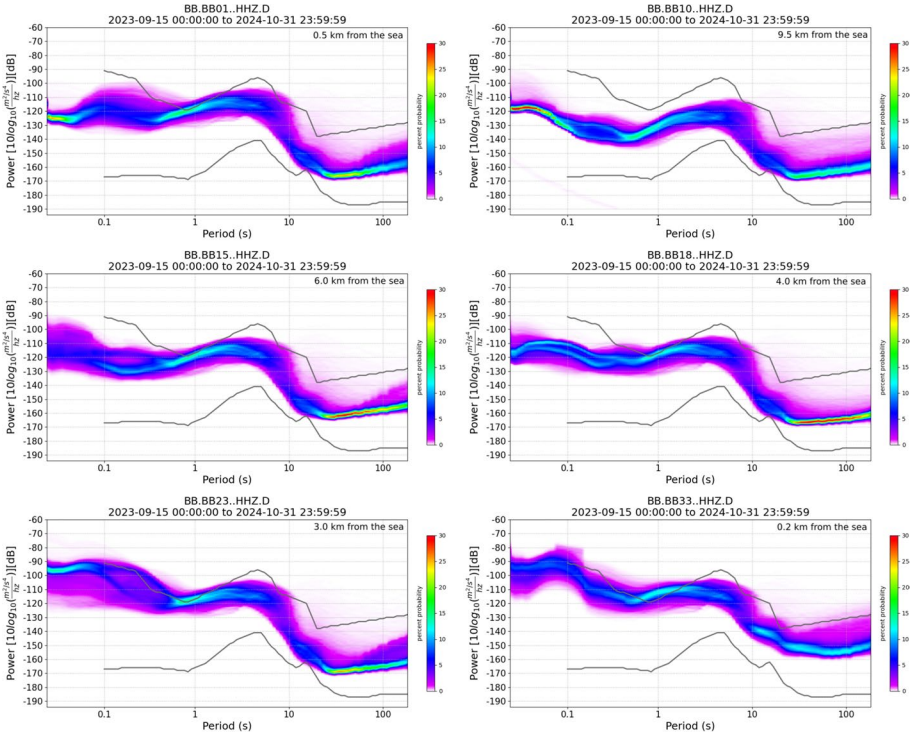

Fig. 10 Examples of PSDs for some stations of the BB network. The grey lines are the new high-noise model (NHNM) and the new low-noise model (NLNM) by Peterson (1993)

seafloor around the island (e.g. Tanimoto and Anderson 2023). The levels of ocean noise in La Palma are elevated, occasionally reaching or exceeding the high-noise reference model. These levels are homogeneous among stations, with a slight decrease towards the island interior (see station BB10 located at the centre of the Caldera de Taburiente). Noise levels are homogeneous at long periods. In contrast, at high frequencies above 1 Hz, noise levels are highly variable among stations. Most of them show two branches in the 2-20 Hz band, corresponding to the day/night cycle of cultural noise. This separation is clearer at stations near towns or roads (e.g. station BB15 near the tunnel crossing Cumbre Nueva, or station BB23 located at the Caños de Fuego Visitor Center), while it is not so evident in the most remote parts of the island (e.g. stations BB01 and BB33 located at the northern and southern tips of La Palma island). The peak at 10-15 Hz observed at station BB33 could be related to the vibrations produced by the operation of windmills in this area.

Figure 11 shows the spatial distribution of seismic noise in La Palma for all stations operating in April 2024, including broadband seismometers and short-period geophones. The map at 0.5 Hz (Fig. 11a) represents the distribution of oceanic microseisms on the island. We observe that the distribution is basically homogeneous, suggesting that the noise levels are similar at all stations as expected for these long-wavelength waves. However, other studies in oceanic volcanic islands have reported subtle spatial gradients associated with proximity to the coastline. For example, Janiszewski et al. (2024) observe an increase in noise levels towards the coast in Hawai'i, particularly at short periods. In contrast, the map at 10 Hz (Fig. 11b) is much more variable. At this frequency, seismic noise is mostly related to cultural activities and atmospheric conditions (i.e. wind) that can change drastically over distances of a few hundred metres. The highest levels of noise are found in coastal areas of the southern half of La Palma, coincident with the most densely populated areas and the most transited roads. The lowest levels occur in the northern half of the island, at the slopes of the Taburiente edifice. Figure 11c shows the variation of the noise

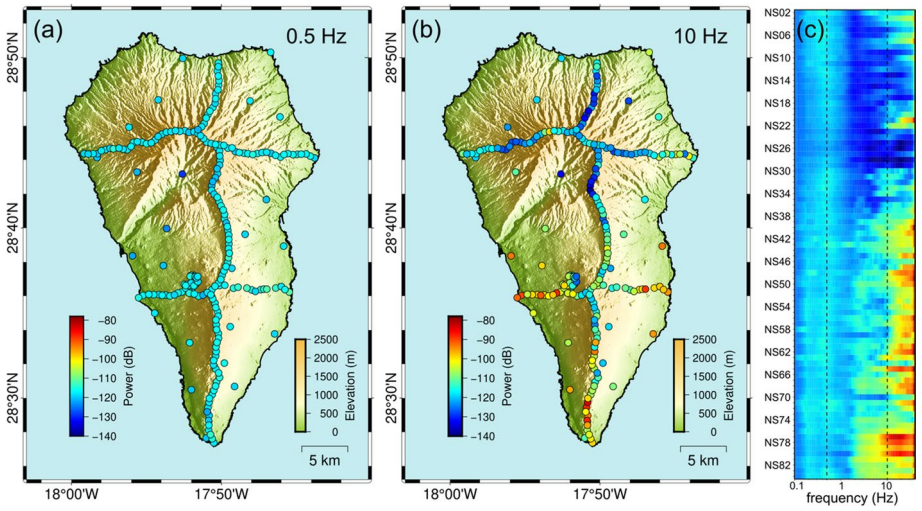

Fig. 11 Representations of the spatial distribution of seismic noise in La Palma from 8 to 23 April 2024. The coloured dots in the maps (**a**) and **b** indicate the average noise power in the vertical component for frequencies of 0.5 Hz and 10 Hz, respectively. Panel **c** shows the average noise power spectra at the stations of the NS profile, using the same colour scale as in the other panels. The vertical dashed lines indicate the frequencies corresponding to the maps shown in (a) and (b)

PSD along the NS profile. Again, we see that the low-frequency part of the PSD is relatively homogeneous, with a small reduction of noise levels near the Caldera de Taburiente (around station NS26). The high-frequency part is more variable, showing again very low levels near the caldera, and a general increase in the noise levels south of station NS40.

4 Preliminary Results

The ~7.5 Tb of raw data (in cube format) obtained during the experiment have been transformed to day-long miniSEED files in a SeisComP3 structure. The dataset was assigned the FDSN network code 7I (2023-2024) and will be available at https://doi.org/10.7914/7w4a-p873 (Almendros et al. 2023). These data are currently only available to project members, but will be open to the scientific community at the end of the embargo period in 2028.

We have begun to exploit the data along different lines. The objectives of the IMAGMASEIS project were mostly related to the application of passive methods based on ambient seismic noise, such as ambient noise tomography and interpretation of H/V ratios. In addition, we will take advantage of the seismicity recorded during the experiment, including teleseisms for receiver function analysis, and local seismicity.

4.1 Ambient Noise

We are working on the analysis of seismic noise for ambient noise tomography, focusing initially on the broadband network. Ambient noise tomography is based on the assumption that Green's functions between station pairs can be retrieved from the cross-correlation of long time series of seismic noise (Shapiro et al. 2005). The first step is to perform cross-correlations of seismic channels to determine dispersion curves and wave velocities. We use MSNoise (Lecocq et al. 2014) to perform the stacked cross-correlations of the vertical components of the BB network broadband stations (Fig. 12a). An example of these stacked cross-correlation is shown in Fig. 12b, between stations BB10 and BB31, from which we can extract the dispersion curve (Fig. 12c) using XDCpick (Ryberg et al. 2021). The analysis of dispersion curves provides measurements of the 2D distribution of surface-wave group velocity at different periods. Preliminary results indicate that the Caldera de Taburiente area is characterised by high group velocities, while the Cumbre Vieja ridge shows low group velocities, especially in the western side. Considering the limited size of the island and commonly adopted sampling criteria in ambient noise tomography, which typically require inter-station distances to exceed about 1.5 times the surface-wave wavelength (e.g. Wilgus et al. 2023), the maximum usable period is constrained by the array aperture and inter-station distances. Given a maximum station separation of approximately 40 km and an average surface-wave velocity of about 3.3 km/s (Cabrera-Pérez et al. 2023), we estimate a maximum usable period of roughly 8 s, which allows imaging down to depths of about 10 km. At shorter inter-station distances, the long recording duration enhances the signal-to-noise ratio of noise cross-correlations, and preliminary results indicate that shorter periods, down to ~0.5 s, can be locally recovered. We expect that the large number of stations (21 permanent and 35 temporary instruments, a total of 56 stations) and global coverage of La Palma will provide a high-resolution image of the structure of the whole island. The comparison with previous models based on data obtained before the 2021

Fig. 12 (**a**) Stacked cross-correlations of the vertical (ZZ) components of all broadband stations with the BB33 station. The traces are band-pass filtered between 0.1 and 1.0 Hz. The coloured lines represent velocities of 3.0 km/s (red), 2.0 km/s (green), and 1 km/s (blue). (**b**) Example of stacked cross-correlation of the vertical component between stations BB10 and BB31, separated by a distance of 23.4 km. The stack was obtained for a period of 11 months. (**c**) Example of dispersion curve analysis of the cross-correlation of the vertical component between stations BB10 and BB31. Traces are normalised in every frequency band. Red colours represent high power, and blue colours represent low power. The dispersion curve is obtained selecting the maximum power for each period

eruption (Cabrera-Pérez et al. 2023, 2024) may provide insights into the changes produced in the shallow structure by the eruptive process.

In addition, we will apply the ambient noise tomography technique to the dense distributions of short-period stations deployed in the IMAGMASEIS experiment. Models of the shallow structure have already been achieved using dense deployments of short-period geophones. For example, Ryberg et al. (2022) applied ambient noise tomography to map velocity anomalies related to mineral exploration in eastern Germany. They used 400 geophones distributed in an area of 1.7×1.1 km with spacing of 70 m and produced a velocity model with good resolution down to a depth of about 500 m. Similarly, Lin et al. (2013) used 5200 stations in California with an average spacing of 100 m to map velocity discontinuities and fault zones to a depth of 1 km. At a larger spatial scale more comparable to our deployment, Wilgus et al. (2023) used ambient noise cross-correlations from an array of approximately 100 stations with ~750 m inter-station spacing to image upper-crustal shear-velocity anomalies beneath a volcanic system. Their analysis focused on periods of a few seconds and provided evidence for magma storage at depths of the order of 10 km, demonstrating the potential of ambient noise tomography to resolve magmatic structures at similar spatial scales. We expect to apply this technique to the most densely covered regions, e.g. the Tajogaite area and the Cumbre Vieja ridge, with the aim of obtaining improved models of the shallow velocity structure.

4.2 Receiver Functions

Another ongoing line of research is the calculation of receiver functions to image the crustal structure, using the teleseisms recorded during the experiment (Fig. 13). Receiver functions are time series obtained by deconvolving the vertical and horizontal components, thus eliminating the source and path effects. Therefore, they are sensitive to the discontinuities of the seismic structure under the receiver (Vinnik 1977; Langston 1979). Although some studies of receiver functions have been performed in the region (Martínez-Arévalo et al. 2013; Ortega-Ramos et al. 2024), the Canary Islands are not particularly well located with respect to the global distribution of large earthquakes to meet the conditions required by receiver function analysis. In our case, the large number of stations and the duration of the experiment ensure the use of multiples teleseisms from different back-azimuths with a global coverage of La Palma. Figure 14 shows an example of the receiver functions calculated at station BB08. The series of pulses are representative of converted seismic phases produced in the main discontinuities of the crustal/upper mantle structure. The combination of the receiver functions obtained by our dense network will allow us to obtain 3D images of the most important discontinuities, including the Moho.

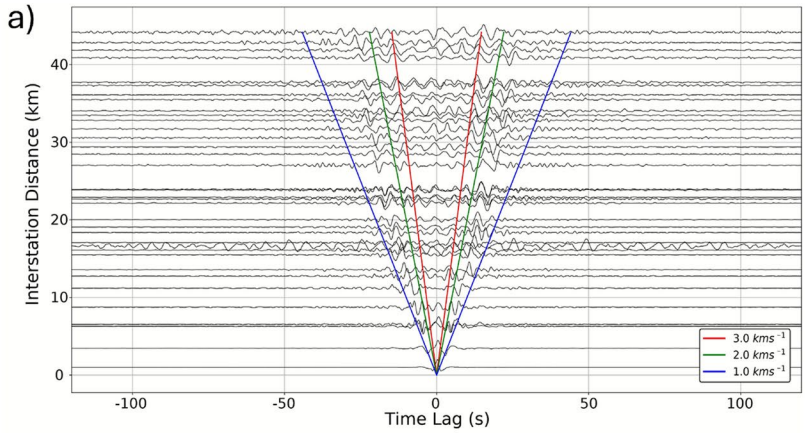
a)
Interstation Distance (km)
Time Lag (s)
3.0 kms⁻¹
2.0 kms⁻¹
1.0 kms⁻¹

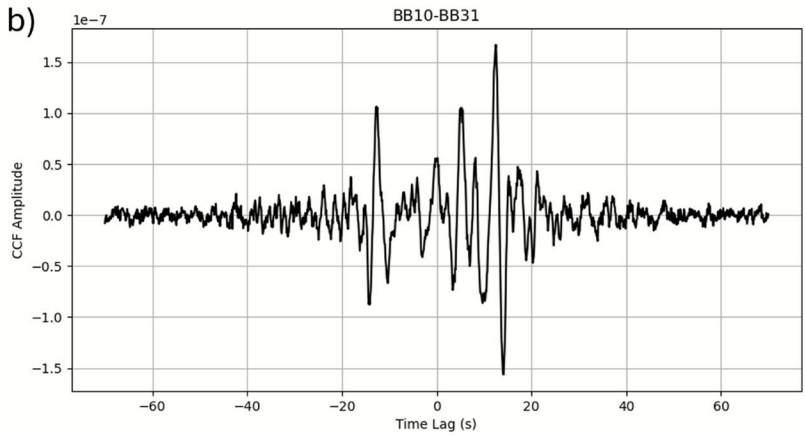
b)
BB10-BB31
1e−7
CCF Amplitude
Time Lag (s)

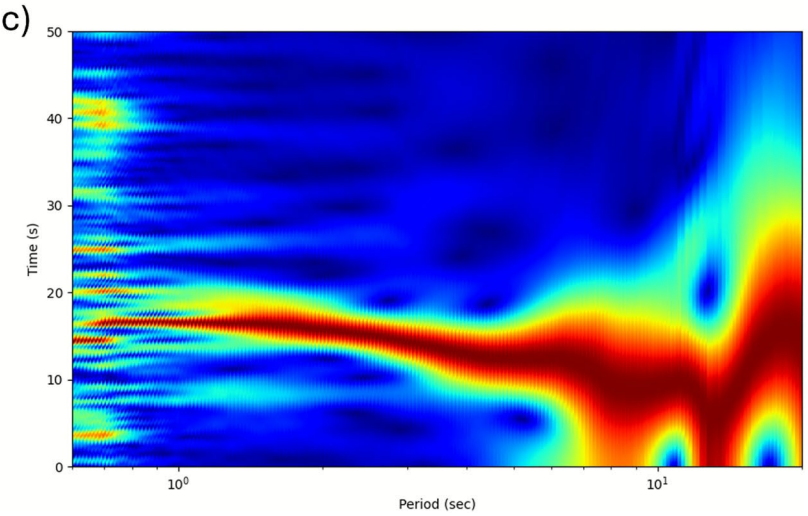
c)
Time (s)
Period (sec)

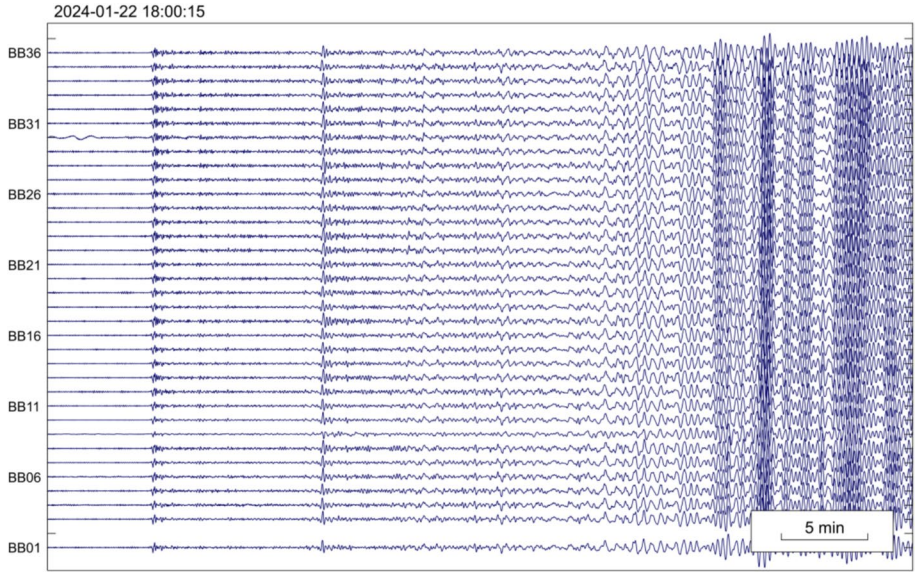

Fig. 13 Example of a teleseism recorded by stations of the BB network. The event occurred at 18:09:04 on 22 January 2024, at the China–Kyrgyzstan border. We show vertical component seismograms filtered in the 1-50 s band

We also plan to apply this method to the geophone stations deployed in our experiment, following the approach of previous studies. For instance, Liu et al. (2018) used teleseismic receiver functions from three nodal profiles in Los Angeles (California) to image the depth and geometry of both the sediment–basement interface and the Moho. Likewise, Lythgoe et al. (2020) employed an 88-station nodal array in Singapore to investigate the crustal structure of the island. In our case, we aim to apply this technique to the three linear profiles and the Cumbre Vieja region, where station density and distribution are optimal for high-resolution imaging.

4.3 Local Earthquakes

We will also perform seismological analyses of the local seismicity recorded during the IMAGMASEIS experiment. Between September 2023 and October 2024, local seismic activity in La Palma was limited. The IGN catalogue reported 172 earthquakes with magnitudes between 0.7 and 2.4 (Instituto Geográfico Nacional 2024). Most of them occurred in the central-western sector of the island, at depths basically limited to the first 10 km of the crust. Despite these low earthquake magnitudes, the high density of seismic stations deployed in our experiment (compared to the sparser configuration of the permanent networks) will allow us to lower the detection and location thresholds. We will expand the catalogue and obtain improved earthquake locations. This can be used to assess the location performance of permanent networks. Moreover, we can characterise the spatial distribution of earthquakes and obtain a sharper image of the seismogenic structures in La Palma. Another challenge will be the calculation of focal mechanisms using the polarity of

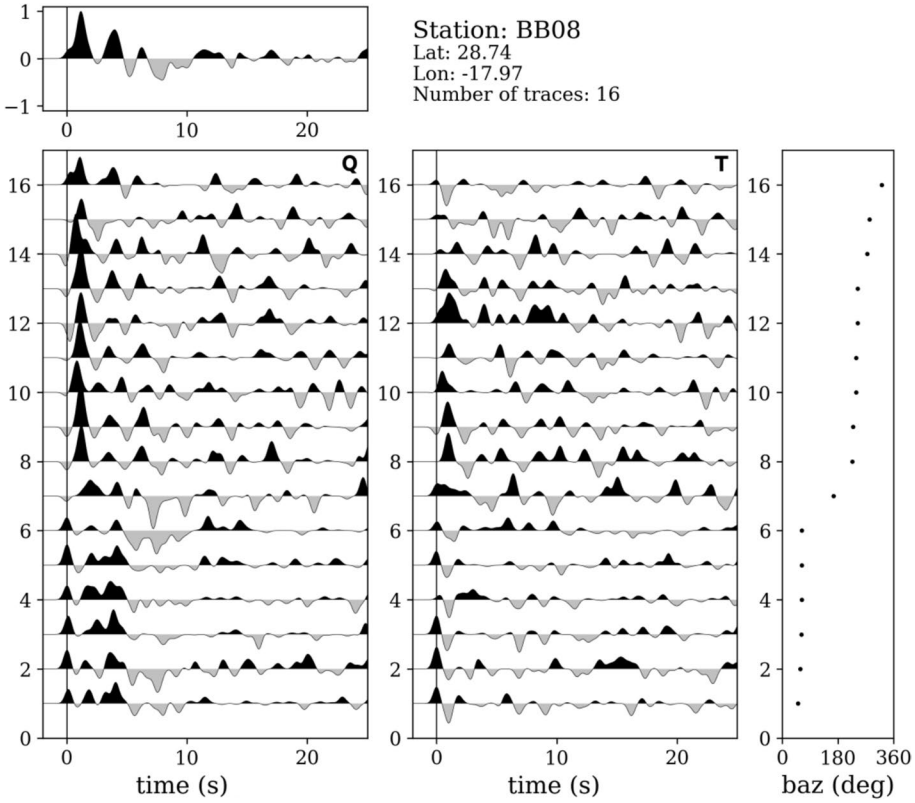

Fig. 14 Example of P-wave receiver functions for the BB08 station. The receiver functions are corrected by PpPms moveout and sorted by back-azimuth (right panel). Q is the rotated radial component respect to incidence angle (left panel), and T is the transversal component (central panel). The Q stack is shown at the top left panel

the first motions. These mechanisms will provide information on the stress distribution in the shallow crust of La Palma.

Figure 15 shows the vertical component waveforms at the stations of the NS profile for a local earthquake recorded in June 2024. This M2.2 earthquake occurred about 3.6 km WSW of Tajogaite volcano, near the southern boundary of the 2021 lava flow, at shallow depths of ~1 km, and was felt in the area with maximum intensity IV. The stations closest to the epicentre are NS51 and NS52 (about 6 km), although the earthquake is still recorded with good signal-to-noise ratio at distances of 25 km towards the north (e.g. station NS02). Interestingly, the signal is less clear towards the south, which may be due either to different noise conditions in this area, or to propagation effects related to the velocity structure under the Cumbre Vieja ridge. In fact, we can identify several anomalies in the relative times and amplitudes of the seismic phases along the profile. These anomalies which will be exploited to investigate the crustal structure.

Figure 16 shows the focal mechanisms of three earthquakes recorded in August 2024. The events on 6 and 28 August were relocated at shallow depths beneath Tajogaite volcano, while the 25 August event occurred at about 4 km SE of Tajogaite, at larger depths (~8 km). The focal mechanisms were estimated using the code FOCMEC included in the

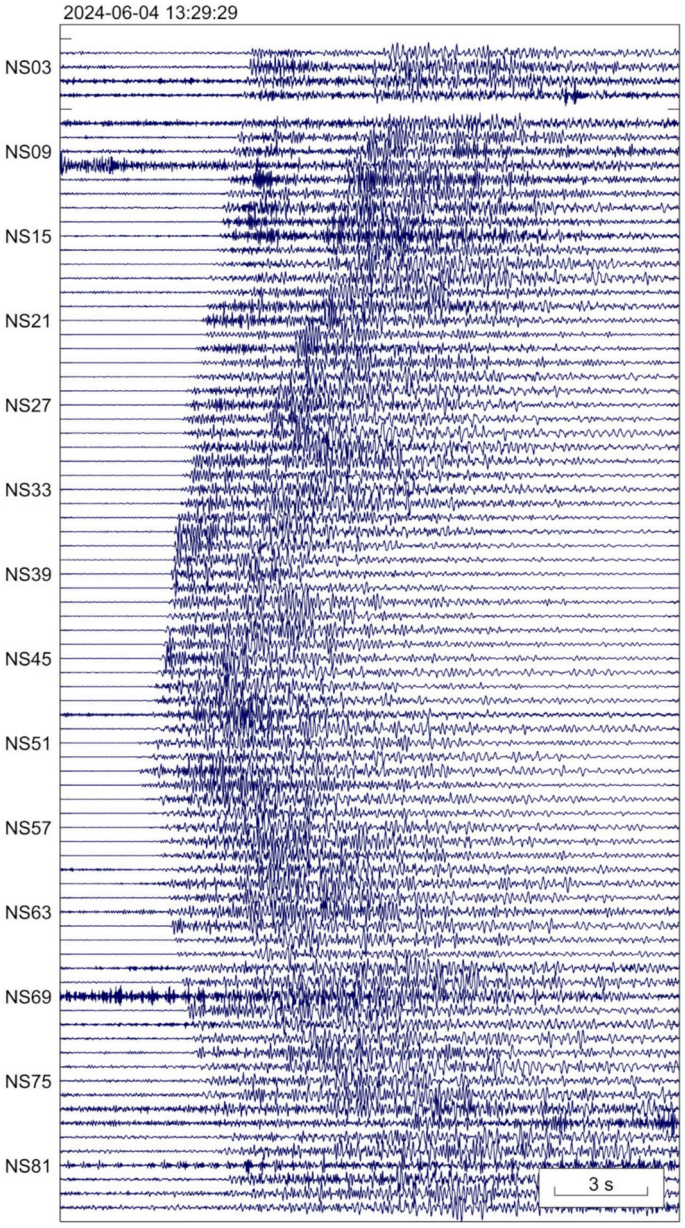

Fig. 15 Example of a local earthquake recorded by the stations of the NS profile on 4 June 2024 at 13:30. We show vertical component seismograms sorted by distance along the profile, from NS01 located in the north coast of La Palma to NS84 in the south

software package SEISAN (Ottemoller et al. 2017). We selected 10-15 well-defined polarities and performed tests to assess the stability of the solutions using different depths and selecting different subsets of polarities. The results suggest that the earthquakes of 25 and 28 August had a strike-slip mechanism, with one of the planes in NE-SW or ENE-WSW

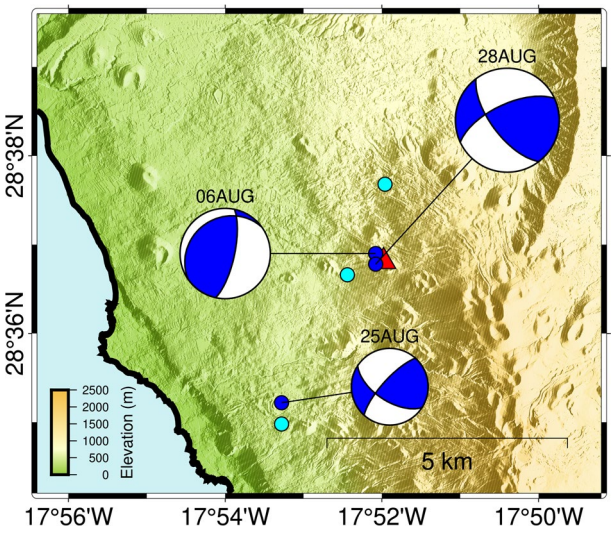

Fig. 16 Example of earthquake locations and focal mechanisms for three of the largest events reported in the IGN catalogue in August 2024. The cyan dots represent the original locations. The blue dots linked to the corresponding focal mechanisms are the IMAGMASEIS relocations. The red triangle indicates the location of Tajogaite volcano

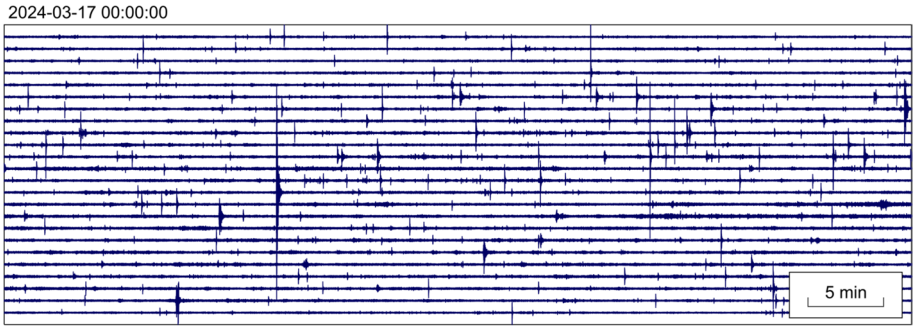

Fig. 17 Example of local seismicity in Tajogaite volcano. We show the vertical component seismogram recorded by station TJ15 of the TJ network on 17 March 2024. Each line corresponds to one hour of data

directions. These directions coincide with the directions of faults mapped in this region (Rodríguez-Pascua et al. 2024). The 6 August event has a mechanism suggesting either a subvertical or a subhorizontal fault. The fact that this earthquake is close to the 28 August event but has a completely different mechanism reveals the complexity of the stress distribution in the Tajogaite area.

Finally, an interesting observation has been the detection of a very large number of very small earthquakes related to the Tajogaite crater area (Fig. 17). Even though more than two years have passed since the end of the eruption, there are still plenty of small earthquakes in the volcanic edifice. These earthquakes were recorded by the TJ network and other nearby stations surrounding the volcanic edifice. Preliminary inspection of the data indicates that there are more than a hundred events per day for the entire recording period of 8 months, which represents many thousands of events. We expect that the large number and density of stations will allow the sources of the earthquakes to be precisely located. These locations will provide insights on the post-eruptive processes occurring within the volcano, such as the effects of cooling and subsidence, the relationship of the seismicity with gas emissions and existing

tectonic structures, and the occurrence of mass movements within the crater. Given the large number of earthquakes, we will use automated methods for the detection and location procedures such as PhaseNet (Zhu and Beroza 2018; Morales et al. 2025). In addition, the resulting catalogue may be used to image the interior of the volcanic edifice using seismic tomography.

5 Conclusions and Perspective

The IMAGMASEIS experiment was carried out in La Palma from September 2023 to October 2024. It consisted of the deployment of a large-N network comprising 35 broadband stations and 200 short-period geophones, deployed in different configurations. These instruments have provided a unique dataset of passive seismic data with unprecedented station density in La Palma. We expect that in the upcoming months and years, the different analyses outlined above will provide high-resolution images of the shallow structure at different scales. These investigations will help us understand the crustal-upper mantle structure, the tectonic regime, the relationship between seismicity and structure, the details of the plumbing system under Cumbre Vieja, the depth and spatial extent of magma accumulation zones, and even the potential of different areas for geothermal exploration. Furthermore, the comparison with studies carried out before the 2021 eruption may lead to a better understanding of the complex structural changes related to the processes of magma emplacement and outbreak. In addition, after all these analyses are complete, the database will be open to the scientific community for further exploitation.

The IMAGMASEIS project is an example of a cost-effective way to characterise the shallow crustal structure in volcanic areas. Large-N deployments are feasible with currently available instruments and technologies. Low-power seismometers and dataloggers combined with the use of slow-discharge batteries allow for the deployment of a large number of stations with very low maintenance. Storage capacity of the dataloggers might be a limitation, but this will be overcome in the near future; for example, the new Datacube3 models already include larger memory cards.

The use of low-weight, slow-discharge batteries has been essential, and it is recommended for deployments with similar durations of around one year. Our large-N deployment would not have been possible if we had used solar panels and standard batteries, which complicates the transport and deployments, lengthens the deployment times, and increases the costs. Apart from these issues, stations powered by solar panels necessarily become conspicuous and cannot be easily camouflaged. Moreover, stations in forests with little direct sunlight would have been problematic.

The application of passive seismological methods based on ambient seismic noise ensures obtaining a velocity model for the region, even if there is no seismicity. These methods can be complemented with other techniques, such as the receiver function analysis based on teleseisms. Furthermore, in volcanic areas there are usually local earthquakes. Even if these earthquakes are just a few, many other analyses can be performed. For example, the large number of earthquakes usually required for travel-time tomography can be balanced out by a large number of seismic stations, given that the crucial parameter is the number and distribution of source-station pairs.

Although the knowledge about volcanoes is rapidly growing, there are still many volcanic areas where the velocity structure is unknown, or just limited to simple 1D models. An adequate knowledge of the 3D velocity structure is fundamental for a correct interpretation of the data provided by monitoring networks. Experiments along the lines

of the IMAGMASEIS project constitute a relatively simple, fast, and cost-effective way to obtain 3D velocity models in volcanic areas where the shallow velocity structure is not well studied.

Supplementary Information The online version contains supplementary material available at https://doi.org/10.1007/s10712-026-09933-y.

Acknowledgements This work has been supported by Grant PID2021-124381NB-C21 funded by MCIN/AEI/ 10.13039/501100011033 and by "ERDF A way of making Europe". The work of J. Tortosa was supported by Grant PRE2022-101370, funded by MCIN/AEI/10.13039/501100011033 and ESF+. Partial support comes also from the Research Group in Seismology and Geophysics (RNM104) of Junta de Andalucía. The instruments used for the IMAGMASEIS network were provided by GFZ (Geophysical Instrument Pool Potsdam, https://www.gfz-potsdam.de/gipp) and by University of Granada (Andalusian Institute of Geophysics, https://iagpds.ugr.es). The success of the project was possible thanks to the close collaboration between scientific institutions, technical staff, local authorities, and inhabitants of the island. We want to thank our colleagues from the Instituto Geográfico Nacional (IGN), Instituto Volcanológico de Canarias (INVOLCAN), and Instituto Geológico y Minero de España (IGME-CSIC) for their support during the experiment and for sharing with us their data, resources, and knowledge about La Palma. We also acknowledge all institutions that have collaborated with our team and helped us achieve our goals, including the Cabildo Insular de La Palma, the Centro de Cooperación Operativa Insular (CECOPIN), the management and agents of the Taburiente Caldera National Park, the Caños de Fuego Interpretation Center, the Volcán de San Antonio Visitor Center, the Juan XXIII School of Tazacorte, and the Town Councils of Fuencaliente, Tijarafe, El Paso, and Puntallana. We thank the local media from La Palma for their interest in our work, which was evidenced in several interviews and notices on social networks. We are very grateful to the people of La Palma, who have let us use their properties to deploy our seismic stations. They generally displayed a definite support for science and a strong curiosity to understand how volcanoes work that arises from the recent 2021 eruption that they all experienced. As an example, we would like to mention Carlos Cecilio Rodríguez López, a good friend who has always been a helping hand and a priceless asset for all the tasks we carried out in the El Paso area. During the planning and deployment phases, we have used digital mapping tools such as OpenStreetMap, Google Maps, Google Earth, Gaia GPS, and OsmAnd. Most figures have been generated using the Generic Mapping Tools (GMT).

Author Contributions The study conception and design were primarily carried out by J. Almendros, X. Yuan, B. Heit, and J. Tortosa. J. Tortosa, E. Carmona, and J. Almendros were responsible for the preparation of the surveys. Field work and data collection were performed by all the authors. Technical and IT support was provided by J. Moreno and M. Á. Dengra. Preliminary data analyses were conducted by J. Tortosa, J. Almendros, J. A. Parera-Portell, E. Carmona, and J. B. Martín. The manuscript was written by J. Tortosa and J. Almendros. All authors read and approved the final manuscript.

Funding Funding for open access publishing: Universidad de Granada/CBUA.

Declarations

Conflict of interest The authors have no conflict of interest to declare that are relevant to the content of this article.

Open Access This article is licensed under a Creative Commons Attribution 4.0 International License, which permits use, sharing, adaptation, distribution and reproduction in any medium or format, as long as you give appropriate credit to the original author(s) and the source, provide a link to the Creative Commons licence, and indicate if changes were made. The images or other third party material in this article are included in the article's Creative Commons licence, unless indicated otherwise in a credit line to the material. If material is not included in the article's Creative Commons licence and your intended use is not permitted by statutory regulation or exceeds the permitted use, you will need to obtain permission directly from the copyright holder. To view a copy of this licence, visit http://creativecommons.org/licenses/by/4.0/.

References

Almendros J, Heit B, Abella R, et al (2023) Deployment of a dense network of broadband and short-period seismometers in La Palma (2023-2024) [Data set]. Network 7I, International Federation of Digital Seismograph Networks https://doi.org/10.7914/7w4a-p873

Cabrera-Pérez I, Soubestre J, D'Auria L et al (2023) Geothermal and structural features of La Palma island (Canary Islands) imaged by ambient noise tomography. Sci Rep 13(1):12892. https://doi.org/10.1038/s41598-023-39910-z

Cabrera-Pérez I, D'Auria L, Soubestre J et al (2024) 3-D intrinsic attenuation tomography using ambient seismic noise applied to La Palma Island (Canary Islands). Sci Rep 14(1):27354. https://doi.org/10.1038/s41598-024-79076-w

Camacho AG, Fernández J, González PJ, et al (2009) Structural results for La Palma island using 3-D gravity inversion. Journal of Geophysical Research: Solid Earth 114(B5). https://doi.org/10.1029/2008JB005628

Carracedo J, Badiola E, Guillou H, et al (2001) Geology and volcanology of la Palma and El Hierro, Western Canaries. Estudios Geologicos-Madrid 57:175–273. https://hal.science/hal-03323419

Civico R, Ricci T, Scarlato P et al (2022) High-resolution Digital Surface Model of the 2021 eruption deposit of Cumbre Vieja volcano, La Palma. Spain Sci Data 9(1):435. https://doi.org/10.1038/s41597-022-01551-8

D'Auria L, Koulakov I, Prudencio J et al (2022) Rapid magma ascent beneath La Palma revealed by seismic tomography. Sci Rep 12(1):17654. https://doi.org/10.1038/s41598-022-21818-9

Day JMD, Troll VR, Aulinas M et al (2022) Mantle source characteristics and magmatic processes during the 2021 La Palma eruption. Earth Planet Sci Lett 597:117793. https://doi.org/10.1016/j.epsl.2022.117793

Dayton K, Gazel E, Wieser P et al (2023) Deep magma storage during the 2021 La Palma eruption. Sci Adv 9(6):eade7641. https://doi.org/10.1126/sciadv.ade7641

Del Fresno C, Cesca S, Klügel A et al (2023) Magmatic plumbing and dynamic evolution of the 2021 La Palma eruption. Nat Commun 14(1):358. https://doi.org/10.1038/s41467-023-35953-y

Di Paolo F, Ledo J, Slezak K et al (2020) La Palma island (Spain) geothermal system revealed by 3D magnetotelluric data inversion. Sci Rep 10(1):18181. https://doi.org/10.1038/s41598-020-75001-z

Díaz J, Villaseñor A, Gallart J et al (2009) The IBERARRAY broadband seismic network: a new tool to investigate the deep structure beneath Iberia. Orfeus Newsl 8(2):1–6

Doran AK, Laske G (2017) Ocean-Bottom Seismometer Instrument Orientations via Automated Rayleigh-Wave Arrival-Angle Measurements. Bull Seism Soc Am 107(2):691–708. https://doi.org/10.1785/0120160165

Gammaldi S, Cabrera-Pérez I, Koulakov I et al (2025) Seismic tomography of a newborn volcano. Geophys Res Lett 52(18):e2025GL114932. https://doi.org/10.1029/2025GL114932

Hansen SM, Schmandt B (2015) Automated detection and location of microseismicity at Mount St. Helens with a large-N geophone array. Geophys Res Lett 42(18):7390–7397. https://doi.org/10.1002/2015GL064848

Heit B, Cristiano L, Haberland C et al (2021) The SWATH-D Seismological Network in the Eastern Alps. Seismol Res Lett 92(3):1592–1609. https://doi.org/10.1785/0220200377

Hetényi G, Molinari I, Clinton J et al (2018) The AlpArray seismic network: a large-scale European experiment to image the Alpine Orogen. Surv Geophys 39:1009–1033. https://doi.org/10.1007/s10712-018-9472-4

Instituto Geográfico Nacional (1999) Spanish Digital Seismic Network [Data set]. Network ES International Federation of Digital Seismograph Networks. https://doi.org/10.7914/SN/ES

Instituto Geográfico Nacional (2024) Catálogo de terremotos. Tech Rep. https://doi.org/10.7419/162.03.2022

Instituto Volcanológico de Canarias (2016) Red Sísmica Canaria [Data set]. Network C7, International Federation of Digital Seismograph Networks https://doi.org/10.7914/SN/C7

Janiszewski H, Bennington N, Wight J (2024) A seismic nodal deployment to understand magmatic structure in the vicinity of the pāhala earthquake swarm. Seismol Res Lett 95(5):3082–3092. https://doi.org/10.1785/0220240060

Langston CA (1979) Structure under Mount Rainier, Washington, inferred from teleseismic body waves. J Geophys Res Solid Earth 84(B9):4749–4762. https://doi.org/10.1029/JB084iB09p04749

Lecocq T, Caudron C, Brenguier F (2014) MSNoise, a Python Package for Monitoring Seismic Velocity Changes Using Ambient Seismic Noise. Seismol Res Lett 85(3):715–726. https://doi.org/10.1785/0220130073

Lin FC, Li D, Clayton RW et al (2013) High-resolution 3D shallow crustal structure in Long Beach, California: Application of ambient noise tomography on a dense seismic array. Geophysics 78(4):Q45–Q56. https://doi.org/10.1190/geo2012-0453.1

Liu G, Persaud P, Clayton RW (2018) Structure of the Northern Los Angeles Basins Revealed in Teleseismic Receiver Functions from Short-Term Nodal Seismic Arrays. Seismol Res Lett 89(5):1680–1689. https://doi.org/10.1785/0220180071

Liu Z, Tian X, Gao R et al (2017) New images of the crustal structure beneath eastern Tibet from a high-density seismic array. Earth Planet Sci Lett 480:33–41. https://doi.org/10.1016/j.epsl.2017.09.048

Longpré MA, Tramontano S, Pankhurst MJ et al (2025) Shifting melt composition linked to volcanic tremor at Cumbre Vieja volcano. Nat Geosci 18(2):175–183. https://doi.org/10.1038/s41561-024-01623-x

Lythgoe KH, Qing Ong Su, M, Wei S (2020) Large-Scale Crustal Structure Beneath Singapore Using Receiver Functions From a Dense Urban Nodal Array. Geophysical Research Letters 47(7):e2020GL087233. https://doi.org/10.1029/2020GL087233

Martí J, Becerril L, Rodríguez A (2022) How long-term hazard assessment may help to anticipate volcanic eruptions: The case of La Palma eruption 2021 (Canary Islands). J Volcan Geotherm Res 431:107669. https://doi.org/10.1016/j.jvolgeores.2022.107669

Martínez-Arévalo C, Mancilla FL, Helffrich G et al (2013) Seismic evidence of a regional sublithospheric low velocity layer beneath the Canary Islands. Tectonophysics 608:586–599. https://doi.org/10.1016/j.tecto.2013.08.021

McNamara DE, Buland RP (2004) Ambient Noise Levels in the Continental United States. Bull Seismol Soc Am 94(4):1517–1527. https://doi.org/10.1785/012003001

Meltzer A, Rudnick R, Zeitler P et al (1999) The USArray initiative. Geol Soc Am Today 9:8–10

Morales J, Dengra MÁ, López-Comino JÁ et al (2025) Fault identification, complexity and evolution of the 2021, Atarfe-Santa Fe earthquake swarm (Granada basin, Spain). Geophys J Int 241(3):1911–1922. https://doi.org/10.1093/gji/ggaf132

NSF Sage (2025) IRIS System for Portable Assessment of Quality (ISPAQ). https://ds.iris.edu/ds/nodes/dmc/software/downloads/ISPAQ/2-0-0/

Ortega-Ramos V, D'Auria L, Granja-Bruña JL et al (2024) Evidence of a low-velocity zone in the upper mantle beneath Cumbre Vieja volcano (Canary Islands) through receiver functions analysis. Geophys Res Lett 51(9):e2023GL105487. https://doi.org/10.1029/2023GL105487

Ottemoller L, Voss P, Havskov J (2017) SEISAN earthquake analysis software for Windows, Solaris, Linux, and MacOSX. http://seis.geus.net/software/seisan/

Peterson J (1993) Observations and modeling of seismic background noise. Open-file Report 93-322, US Geological Survey, https://doi.org/10.3133/ofr93322

Prieto JF, González PJ, Seco A et al (2009) Geodetic and structural research in La Palma, Canary Islands, Spain: 1992–2007 results. Pure Appl Geophys 166:1461–1484. https://doi.org/10.1007/s00024-009-0505-2

Przeor M, Castaldo R, D'Auria L et al (2024) Geodetic imaging of magma ascent through a bent and twisted dike during the Tajogaite eruption of 2021 (La Palma, Canary Islands). Sci Rep 14(1):212. https://doi.org/10.1038/s41598-023-50982-9

Rodríguez-Pascua MA, Pérez-López R, Perucha MA, et al (2024) Active faults, kinematics, and seismotectonic evolution during Tajogaite eruption 2021 (La Palma, Canary Islands, Spain). Applied Sciences 14(7). https://doi.org/10.3390/app14072745

Romero Ruiz MC (1990) Las manifestaciones volcánicas históricas del Archipiélago Canario. PhD thesis, PhD Thesis, University of La Laguna, Spain

Romero-Toribio MC, Martín-Hernández F, Ledo J (2025) High-resolution drone-based aeromagnetic survey at the tajogaite volcano (la palma, canary islands): Insights into its early post-eruptive shallow structure. Remote Sens 17(18):3153. https://doi.org/10.3390/rs17183153

Ryberg T, Haberland C, Green RG et al (2021) A fast gui-based tool for group-velocity analysis of surface waves. Seismol Res Lett 92(4):2640–2646. https://doi.org/10.1785/0220200425

Ryberg T, Kirsch M, Haberland C et al (2022) Ambient seismic noise analysis of large-N data for mineral exploration in the Central Erzgebirge. Ger Solid Earth 13(3):519–533. https://doi.org/10.5194/se-13-519-2022

Serrano I, Dengra MA, Almendros J et al (2023) Seismic anisotropy tomography beneath La Palma in the Canary Islands. Spain J Volcan Geotherm Res 441:107870. https://doi.org/10.1016/j.jvolgeores.2023.107870

Shapiro NM, Campillo M, Stehly L et al (2005) High-resolution surface-wave tomography from ambient seismic noise. Science 307(5715):1615–1618. https://doi.org/10.1126/science.1108339

Tanimoto T, Anderson A (2023) Seismic noise between 0.003 Hz and 1.0 Hz and its classification. Prog Earth Planet Sci 10(1):56. https://doi.org/10.1186/s40645-023-00587-7

Torres-González PA, Luengo-Oroz N, Lamolda H et al (2020) Unrest signals after 46 years of quiescence at Cumbre Vieja, La Palma. Canary Islands J Volcan Geotherm Res 392:106757. https://doi.org/10.1016/j.jvolgeores.2019.106757

Tortosa J (2023) Análisis de la sismicidad en La Palma tras la erupción de 2021 mediante técnicas de array. Master's thesis, MSc Thesis, University of Granada, Spain, https://hdl.handle.net/10481/93594

Troll VR, Carracedo JC (2016) The geology of the Canary Islands. Elsevier. https://doi.org/10.1016/C2015-0-04268-X

Vinnik L (1977) Detection of waves converted from p to sv in the mantle. Phys Earth Planet Inter 15(1):39–45. https://doi.org/10.1016/0031-9201(77)90008-5

Wilgus J, Schmandt B, Maguire R et al (2023) Shear velocity evidence of upper crustal magma storage beneath valles caldera. Geophys Res Lett 50(5):e2022GL101520. https://doi.org/10.1029/2022GL101520

Zhu W, Beroza GC (2018) Phasenet: a deep-neural-network-based seismic arrival-time picking method. Geophys J Int 216(1):261–273. https://doi.org/10.1093/gji/ggy423

Publisher's Note Springer Nature remains neutral with regard to jurisdictional claims in published maps and institutional affiliations.

Authors and Affiliations

Javier Tortosa[1,2] · Javier Almendros[1,2] · Enrique Carmona[2] · José Benito Martín[2] · Janire Prudencio[1,2] · Joan Antoni Parera-Portell[1,2] · Rafael Abella[3] · Carlos Araque-Pérez[1,2] · José Morales[1,2] · Pablo Rey-Devesa[1,2] · Benjamin Heit[4] · Xiaohui Yuan[4] · Alfonso Ontiveros-Ortega[5] · Iván Melchor[6] · Cinthia Guerrero-Reinoso[1,2] · David Carrero[2] · Inmaculada Serrano[1,2] · Gerardo Alguacil[1,2] · Guillermo Cortés[1,2] · Mercedes Feriche[2] · Antonio Martos[2] · Javier Moreno[2] · Miguel Ángel Dengra[2]

✉ Javier Tortosa
javitsg@ugr.es

[1] Departamento de Física Teórica y del Cosmos, University of Granada, Granada, Spain

[2] Instituto Andaluz de Geofísica, University of Granada, Granada, Spain

[3] Instituto Geográfico Nacional, Madrid, Spain

[4] GFZ German Research Centre for Geosciences, Postdam, Germany

[5] University of Jaén, Jaén, Spain

[6] Universidad Nacional de Río Negro - CONICET, General Roca, Argentina